EDGE ARTICLE

Check for updates

All publication charges for this article have been paid for by the Royal Society of Chemistry

A metal-free 2D layered organic ammonium halide framework realizing full-color persistent room-temperature phosphorescence†

Shangwei Feng,‡ Qiuqin Huang,‡ Shuming Yang, Zhenghuan Lin [ID] *
and Qidan Ling [ID]

Organic–inorganic hybrid metal halides have attracted intensive attention because of their unique electronic structure and solution processability. They have a rigid micro/nano-structure and heavy atom effect, which has obvious advantages in promoting organic room temperature phosphorescence (RTP). However, the toxicity of heavy metals has limited their further development. Herein, two metal-free 2D layered ammonium halides, homopiperonylammonium bromide and chloride (HLB and HLC), are described for the first time. Their layered structure consists of rigid inorganic ammonium halide laminates and neatly stacked organic layers. The rigid laminates and external heavy atom effect of halogen atoms make HLB and HLC produce green RTP. When phosphor guests with different triplet energies are doped into HLB, HLC, or phenylethylamine salt hosts, effective full-color and even white ultra-long RTP with phosphorescence quantum yield up to 18.7% and lifetime up to 1.7 s is realized through energy transfer between the host and guest. Due to the simple solution synthesis, 10 g-level doped layered organic ammonium halides with the same phosphorescence properties can be easily obtained. The information ink based on these doped halides and non-toxic ethanol solvent can form various patterns on filter paper. The fluorescence and phosphorescence of these patterns are sensitive to the excitation wavelength and acid–base vapor. Consequently, they can be applied to multiple complex anti-counterfeiting and fluorescence/phosphorescence dual-mode chemical sensors.

Introduction

Organic room temperature phosphorescence (RTP), especially ultralong-lived organic phosphorescence (UOP), has gradually become a research hotspot because of its potential applications in emerging fields such as intelligent information encryption, optical anti-counterfeiting, biological imaging and so on.[1–6] However, the triplet excitons produced through intersystem crossing (ISC) are extremely sensitive to moisture and oxygen, so the phosphorescence quantum yield (Φ_P) of UOP materials is usually low in air.[3,7–9] The main research strategies to improve the quantum yield and lifetime of phosphorescence include crystal engineering, host–guest interaction, spatial confinement and introducing the weak force of heteroatoms.[10–15] In general, these methods mainly improve the phosphorescence performance from two aspects. One is to promote ISC and increase the number

of triplet excitons by introducing heteroatoms such as aromatic carbonyl groups, heavy atoms, oxygen or nitrogen.[9,16] The second is to create a rigid oxygen-free environment, inhibit the movement of organic luminophores, and reduce the probability of non-radiative deactivation of triplet excitons.[17,18] Among them, the internal heavy atom effect produced by directly introducing halogen atoms into the luminescent group is one of the most effective methods to increase the rate of ISC and improve the phosphorescence efficiency.[19,20] However, the internal heavy-atom effect (HAE) also accelerates the phosphorescence process, reducing the phosphorescence lifetime (τ).[9,21,22] Therefore, it is not easy to obtain UOP with high Φ_P and long τ.

When heavy atoms or ions coexist with phosphors, they may have intermolecular electronic coupling or coordination interactions with phosphors. This external HAE is expected to improve the efficiency and lifetime of RTP at the same time.[12,23–28] For example, Lu *et al.*[25] synthesized a series of carbazole derivatives containing bromine atoms connected by flexible alkyl chains. It was found that the RTP efficiency depends on the distance between the bromine atom and carbazole, and the weak intermolecular interaction. It is worth noting that when a 6-(4-bromophenoxy)hexyl group is connected with carbazole, a Φ_P of 39.5% and RTP lifetime of 200 ms can be realized. Lin *et al.*[26] doped a naphthalimide phosphor

into a 2D layered organic–inorganic perovskite based on lead bromide and lead chloride to obtain two doped perovskites, PEPB–NIA and PEPC–NIA, respectively. Due to the external HAE of Br and Pb, PEPB–NIA showed efficient yellow RTP of naphthalimide (Φ_P = 25.6%, τ = 6.3 ms). Compared with PEPB–NIA, the PbCl$_2$-based perovskite PEPC–NIA showed higher RTP Φ_P (56.1%) and a longer lifetime (35 ms) with a yellow afterglow. To avoid the toxicity and too strong HAE of Pb, they also doped the naphthalimide into a layered organic–inorganic zinc bromide (PEZB).[27] The RTP lifetime of naphthalimide was improved from 6.3 ms in the hybrid PbBr$_2$ perovskite to 102 ms in the hybrid PEZB. In particular, when another organic phosphor based on naphthalene was assembled into the laminate of PEZB, the lead-free hybrid showed stable and persistent RTP emission (τ > 150 ms, Φ_P = 42% in crystals; Φ_P = 27% in films) in air. For organic afterglow materials with a lifetime longer than 100 ms, the quantum yields in both crystals and films were the highest values reported at that time. These results show that a moderate external HAE can regulate the phosphorescence properties of organic phosphors, and simultaneously improve the phosphorescence quantum yield and lifetime.

However, metal ions, especially heavy metal ions, are not friendly to the environment.[29,30] Therefore, the development of metal-free UOP materials with an external HAE is of great significance. Herein, we obtain a kind of new metal-free organic ammonium halide based on 3,4-methylenedioxyphenylamine (HLA) characterized by a unique 2D layered structure which endows it with excellent optical properties. Both the hydrobromide and hydrochloride of HLA, named HLB and HLC, exhibit strong fluorescence at 322 nm and RTP at around 530 nm with lifetime up to 79 ms. Interestingly, when HLB and HLC are employed as hosts (Fig. 1), effective UOP with Φ_P up to 18.7% and lifetime up to 1.0 s can be achieved by doping guest ammonium salts based on naphthalene, 1,8-naphthalimide, 2,3-naphthalimide and pyrene, due to effective energy transfer between the host and guest. The afterglow colour can be tuned from green (482 nm) to red (679 nm). When the phenylethyl ammonium halide with the same 2D structure and a higher singlet energy level is selected as the host, and doped with ammonium salts containing biphenyl and 1,8-naphthalimide,

a blue and white afterglow with τ up to 1.7 s is obtained. Because of the use of environmentally friendly ethanol as solvent, and the absence of heavy metals, these organic eutectics have great application potential in safety ink and information anti-counterfeiting.

Results and discussion

Two organic ammonium halides, HLB and HLC, were easily obtained in high yield of more than 95%, from a 3,4-methylenedioxyphenethylamine solution in ethyl acetate through adding HCl or HBr. To avoid the effect of impurity on their luminescence properties, HLB and HLC powders were further purified by recrystallization in hot alcohol solution. The structure of HLB and HLC crystals was confirmed by NMR and single-crystal X-ray diffraction (SC-XRD). Their single molecular conformation is shown in Fig. S1† with structure refinement data summarized in Table S1.† The detailed layered packing mode of HLB and HLC is shown in Fig. 2. It was found that they present a unique two-dimensional layered structure. An inorganic ammonium halide (–NH$_3$Br or –NH$_3$Cl) forms a rigid laminate, while organic 1,3-benzodioxole rings are arranged on both sides of the laminate. However, the packing mode of 1,3-benzodioxole rings is different in HLB and HLC crystal lattices, respectively, presenting parallel and wavy shapes (Fig. 2c and d). Every molecule is fixed in the lattice through various interactions existing in both the inorganic ammonium salt and organic aromatic ring layers (Fig. S2 and S3†). Taking HLB as an example, there are mainly three kinds of hydrogen bonding between Br and ammonium ions with the distance of short contact (Br$^-$···H$^+$) at about 2.503 Å in the inorganic laminate, while the other two kinds of weak interaction, O···O (3.033 Å) and O···H (2.801 Å and 2.507 Å), are found between two organic layers. These interactions can effectively inhibit molecular
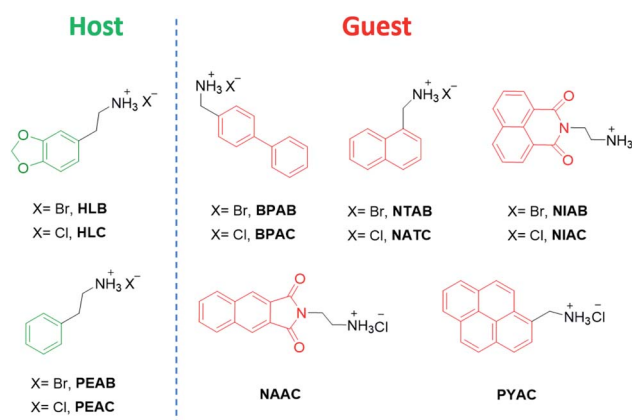

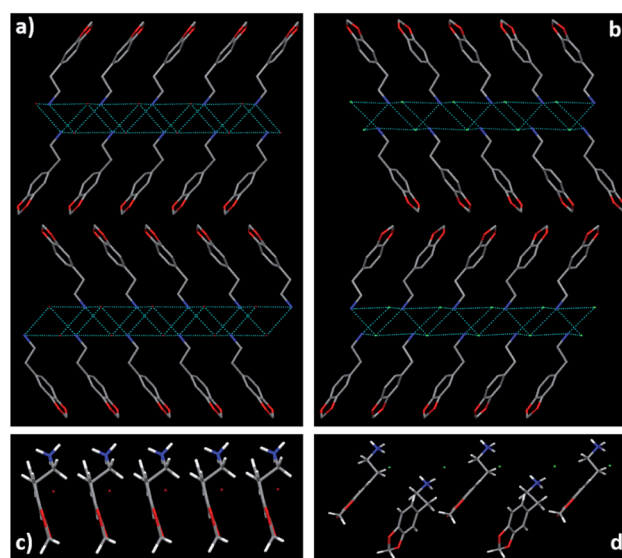**Fig. 1** Molecular structure of host and guest ammonium halides.

Fig. 2 2D layered structure of HLB (a) viewed from the c axis and HLC (b) viewed from the *a* axis. 1D alignment of organic molecules in HLB (c) along the *b* axis and HLC (d) along the *c* axis.
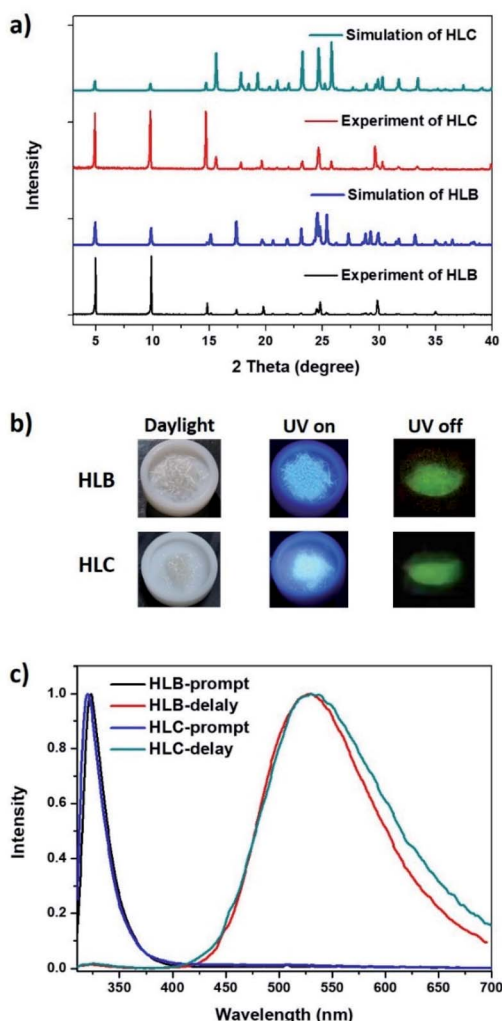
Fig. 3 (a) Simulated and experimental PXRD patterns of HLB and HLC crystals. (b) Photos of HLB and HLC crystals under a daylight lamp and a UV lamp of 365 nm. (c) Prompt and delay emission spectra of HLB and HLC crystals (λ_{ex} = 300 nm).

movement, which is helpful for luminescence of HLB molecules. Powder X-ray diffraction (PXRD) analysis of HLB and HLC shows identical diffraction patterns to their simulated ones, which confirms that their crystalline structures are pure and homogeneous (Fig. 3a). There are mainly (h00) diffraction peaks in the PXRD patterns of HLB and HLC, which are caused by their 2D layered structure. HLB and HLC crystals show high thermal stability with the 5% weight-loss temperature at 310 °C and 234 °C, respectively (Fig. S4†).

The resulting white crystals exhibit blue luminescence under 365 nm UV light with high power (Fig. 3b). After turning off the UV light, HLB and HLC crystals show a green afterglow. From the prompt and delay luminescence spectra of HLB and HLC (Fig. 3c), it was found that their fluorescence emission peaks are at around 320 nm, and that the phosphorescence emission bands locate at around 530 nm. The excitation spectra of HLB and HLC monitored at 320 nm show maximum excited peaks at about 300 nm, while their excitation bands monitored at 530 nm are in the range between 300 nm and 400 nm (Fig. S5†).

It suggests that the fluorescence and phosphorescence of HLB and HLC are derived from different emissive centers. Their emission peaks in dilute ethanol solution are at 318 nm and close to 320 nm (Fig. S6†). Consequently, it can be inferred that the fluorescence of HLB and HLC has originated from the single-molecule state. However, the delay spectrum of HLB dilute solution at 77 K shows that the emission peak of single molecule phosphorescence is at 472 nm (Fig. S7†), which is very different from the phosphorescence emission peak (530 nm) of the HLB or HLC crystal. Consequently, phosphorescence of HLB and HLC crystals originated from the aggregated state rather than the single molecule state. The luminescence quantum yields of HLB and HLC crystals were measured to be 15% and 19%, respectively. The transient luminescence decay plots of HLB and HLC monitored at fluorescence and phosphorescence peaks are shown in Fig. S8.† Based on the decay plots, the lifetime of singlet excitons was fitted to be 3.1 ns, while the lifetime of triplet excitons was calculated to be 26.23 ms (for HLB) and 79.25 ms (for HLC). The longer RTP lifetime of HLC than HLB likely originated from the weaker HAE of Cl than Br.

To obtain colorful RTP materials with a high quantum yield and ultralong lifetime, different ammonium salts based on phosphors were employed as guests (Fig. 1) and doped into the HLB or HLC host (Fig. 4a). Förster energy transfer (ET) was expected to occur between the host and guest, and yield highly efficient RTP of guests (Fig. 4b). Firstly, three organic ammonium bromides based on biphenyl (BPAB), naphthalene (NTAB) and 1,8-naphthalimide (NIAB) were respectively doped into HLB to obtain single-molecule blue, green and yellow UOP of guests.[27] The doping ratio of the three ammonium salts (BPAB, NTAB and NIAB) was controlled at 1%. However, the prompt and delay emission peaks of the HLB–BPAB doped salt are respectively at 323 nm and 520 nm, which should belong to the fluorescence and phosphorescence of HLB rather than BPAB (Fig. S9a†). BPAB displays a blue single-molecule RTP peak at 475 nm with two shoulders, as reported previously.[27,31] Meanwhile, HLB–NTAB and HLB–NIAB exhibit green and yellow RTP at 509 nm and 586 nm (Fig. S9b and c†), corresponding to their single-molecule phosphorescence, respectively.[27,32] However, the intensity of green RTP of HLB–NTAB is lower than that of HLB–NIAB. It seems that the ET efficiency between the guest and HLB host increases gradually in the order of HLB–BPAB, HLB–NTAB, and HLB–NIAB. From Fig. S10,† it was found that the absorption band of BPAB dilute solution locates before 300 nm. Due to the absorption mismatching with the emission of HLB (above 300 nm), there is no Förster ET between HLB and BPAB. That is why HLB–BPAB did not exhibit blue UOP of biphenyl. The overlapping area of NIAB absorption with HLB emission is larger than that of NTAB. As a result, the ET efficiency is higher in HLB–NIAB than HLB–NTAB. There should be almost no Dexter energy transfer existing in the doping system based on the following aspects. Firstly, triplet excitons of HLB or HLC are very few, because no phosphorescence peak appears in their prompt emission spectra (Fig. 3c). Secondly, the triplet state energy of BPAB is close to that of HLB; however, phosphorescence of BPAB was not found in HLB–BPAB (Fig. S9a†). Thirdly, the energy transfer efficiency between the guest and
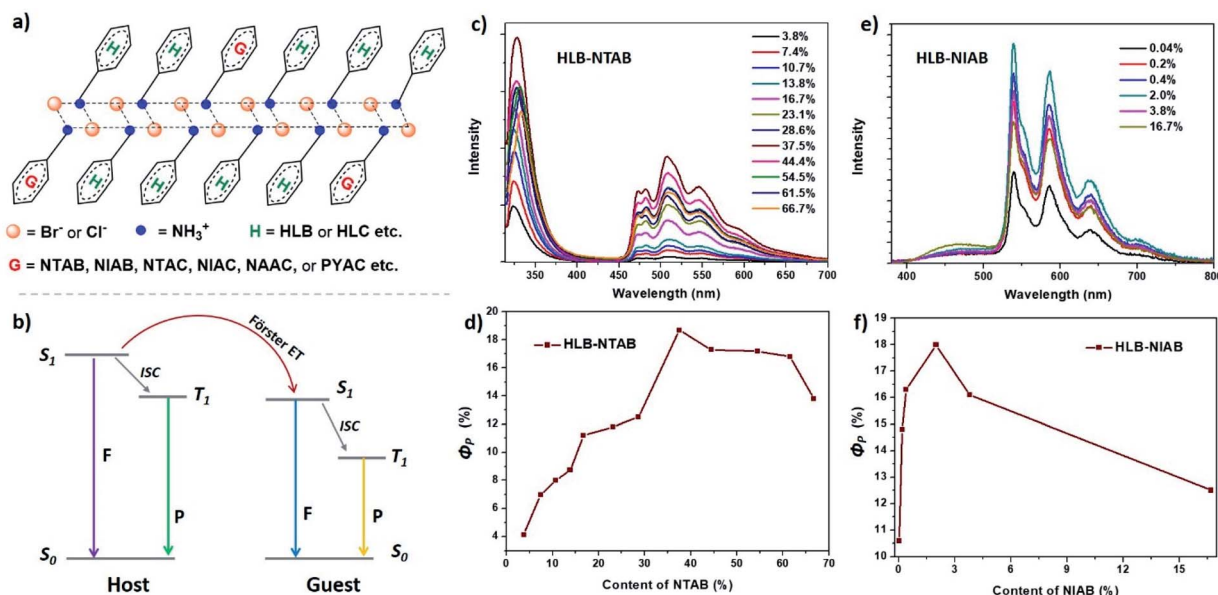
Fig. 4 (a) Structure diagram of the host−guest system. (b) Possible energy transfer mechanism existing in the host−guest system: P = phosphorescence; F = fluorescence. Effect of NTAB loading amount on emission spectra (c and e) and phosphorescence quantum yield (d and f) of HLB−NTAB (c and d) and HLB−NIAB (e and f).

host in the doped HLB strongly depends on the overlapping area of the absorption band of the guest and the emission band of the host (Fig. S10†).

The doping ratio of NTAB and NIAB was changed to realize the strongest RTP emission. Fig. 4c shows that the maximum RTP intensity of HLB−NTAB appears at a doping ratio of 37.5%, corresponding to Φ_P of 18.7% (Fig. 4d), while the strongest RTP emission of HLB−NIAB with 18.0% Φ_P appears at a doping ratio of 2.0% (Fig. 4e and f). As previously mentioned, the ET efficiency in HLB−NIAB is higher than that in HLB−NTAB. As a result, a lower doping ratio of HLB−NIAB than HLB−NTAB realizes the strongest RTP. The lifetime of RTP at 509 nm (for HLB−NTAB) and 586 nm (for HLB−NIAB) was calculated to be 71.3 ms and 223.5 ms from transient luminescence decay plots (Fig. S11†). The photophysical data have been summarized in Table 1. The PXRD patterns of HLB−NTAB and HLB−NIAB exhibiting similar diffraction peaks to those of HLB confirm their 2D layered structure (Fig. S12a†). It should be noted that

a feed ratio of 37.5% for NTAB in HLB does not destroy the 2D layered structure of HLB. Additionally, the delay spectrum of NTAB dilute solution at 77 K shows a broad emissive band centered at 506 nm (Fig. S13†), which indicates that the RTP of HLB−NTAB originated from the triplet state of the single molecule guest. We speculate that the actual doping ratio may be far lower than the theoretical doping ratio, because a low doping ratio will not destroy the two-dimensional layered structure of HLB. To confirm the speculation, the NMR spectrum of HLB−NTAB (37.5% feed ratio) in d-DMSO was measured. From the ^{1}H NMR spectrum (Fig. S14†), the actual amount of NTAB in HLB−NTAB can be estimated to be 2% from the integral value of hydrogen of methylene, which is far from the loading amount of 37.5%. Such a big difference should be attributed to the fact that HLB has low solubility in ethanol solvent, while NTAB has high solubility in ethanol solvent. When the hot ethanol solution of HLB and NTAB is cooled to room temperature, most of the HLB and a small amount of

Table 1 Photophysical properties of 2D ammonium halides doped with different luminophores

| | Doping content[a] (%) | λ_{ex} (nm) | Fluorescence | | Phosphorescence | | | |
			λ_{em} (nm)	τ (ns)	λ_{em} (nm)	τ (ms)	Φ_P (%)	$\Phi_t{}^{b}$
HLB−NTAB	37.5	310	328	2.06	509	71.3	18.7	26.6
HLB−NIAB	2.0	340	—	—	586	223.5	18.0	18.7
HLC−NTAC	20.0	305	328	7.3	510	522.0	3.9	15.9
HLC−NIAC	2.4	340	470	11.39	586	328.8	8.3	10.2
HLC−NAAC	2.4	365	445	7.06	525	979.3	5.1	6.8
HLC−PYAC	0.5	350	380	93.8	679	217.1	3.0	36.7
PEAB−BPAB	3.8	288	311	14.0	477	437.0	9.9	26.6
PEAC−BPAC	3.8	294	304	35.6	478	1726	1.4	18.7

^{a} Theoretical value. ^{b} Φ_t is the total quantum yield.

NTAB begin to form crystals. Therefore, only a small amount of NTAB enters the lattice of HLB, resulting in an actual doping ratio of 2%, although the feed ratio of NTAB is 37.5%.

Then, four organic ammonium chlorides based on naphthalene (NTAC), 1,8-naphthalimide (NIAC), 2,3-naphthalimide (NAAC) and pyrene (PYAC) were employed as guests doped into HLC to obtain colorful RTP with longer lifetimes, due to the weaker HAE of Cl than Br. The obtained salts (HLC–NTAC, HLC–NIAC, HLC–NAAC and HLC–PYAC) also exhibit a 2D layered structure inferred from the identical PXRD patterns with HLC (Fig. S12b†). As expected (Fig. 5 and S15†), these doped chlorides display a colorful afterglow with the phosphorescence emission bands ranging from 510 nm to 679 nm. Compared with HLB–NTAB and HLB–NIAB, HLC–NTAC and HLC–NIAC show longer RTP lifetimes (Fig. S16†). In particular, the RTP lifetime of HLC–NTAC is nearly 7.3 times longer than that of HLB–NTAB (Table 1). However, these salts based on ammonium chlorides show relatively low Φ_P due to the weak heavy atom effect of Cl. Among these salts, HLC–NAAC gives the longest RTP lifetime of around 1 s with more than 10 s of afterglow (Fig. 5c). The Φ_P of HLC–NAAC is 5.1% which is greater than that of most UOP materials with lifetime longer than 1 s.[3,7,33–36] Interestingly, a white emission was found upon exciting HLC–NIAC with 365 nm UV light. The white emission originated from the matched fluorescence and phosphorescence with comparable intensity at 470 nm and 586 nm, respectively (Fig. S15b†). The CIE 1931 chromaticity coordinates of HLC–NIAC were calculated to be (0.33, 0.39) which are close to those of standard white light (0.33, 0.33). Consequently, HLC–NIAC is a potential single-component luminescent material for UV-driven white light-emitting devices (UV-WLEDs) with an afterglow, which is beneficial for protecting our eyes when abruptly turning off the power at night.[37]

To obtain the blue UOP of BPAB, another ammonium bromide based on phenylethylamine (PEAB) was selected as its host (Fig. 1). Förster ET was expected to occur between PEAB and BPAB, because PEAB shows high energy emission at 286 nm matching the absorption of BPAB (Fig. S17a†). As shown in Fig. 5a and S17b and c,† PEAB–BPAB does show a blue afterglow with phosphorescent emission at 477 nm and lifetime of 437 ms. PEAC–BPAC, a chloride counterpart of PEAB–BPAB, also displays a blue RTP with an ultralong lifetime up to 1726 ms (Fig. S18†). Based on the blue afterglow of PEAB–BPAB, a white afterglow, which is difficult to realize,[38,39] can be expected through incorporating blue and yellow afterglow guests into PEAB. NIAC was chosen as a yellow afterglow guest because its lifetime (329 ms) is relatively close to that of BPAB (437 ms). Consequently, NIAC and BPAB were co-doped into PEAB to give a three-component ammonium salt, PEAB–BPAB–NIAC. For both prompt and delay spectra, the emission band covers the total visible light range of 400–700 nm (Fig. S19†). Interestingly, under a UV lamp, PEAB–BPAB–NIAC exhibits a warm white light with CIE of (0.33, 0.41) and CCT of 5578 K, while it shows a cold white afterglow with CIE of (0.29, 0.38) and CCT of 6995 K after turning off the UV lamp (Fig. 5a).

The large-scale production of materials is very important for practical application. Because metal-free 2D halides are smoothly synthesized without harsh experimental conditions and complex equipment, it is easy to realize their large-scale production. HLC–NAAC was selected for a batch production test at the 10 g level due to its long lifetime (around 1 s) and decent phosphorescence quantum yield (larger than 5%). As shown in Fig. 6a, more than 11 g of HLC–NAAC was successfully synthesized, displaying 10 s of green afterglow. It shows an identical phosphorescence emission band and lifetime to those of the small-scale counterpart (Fig. S20†). High luminescence
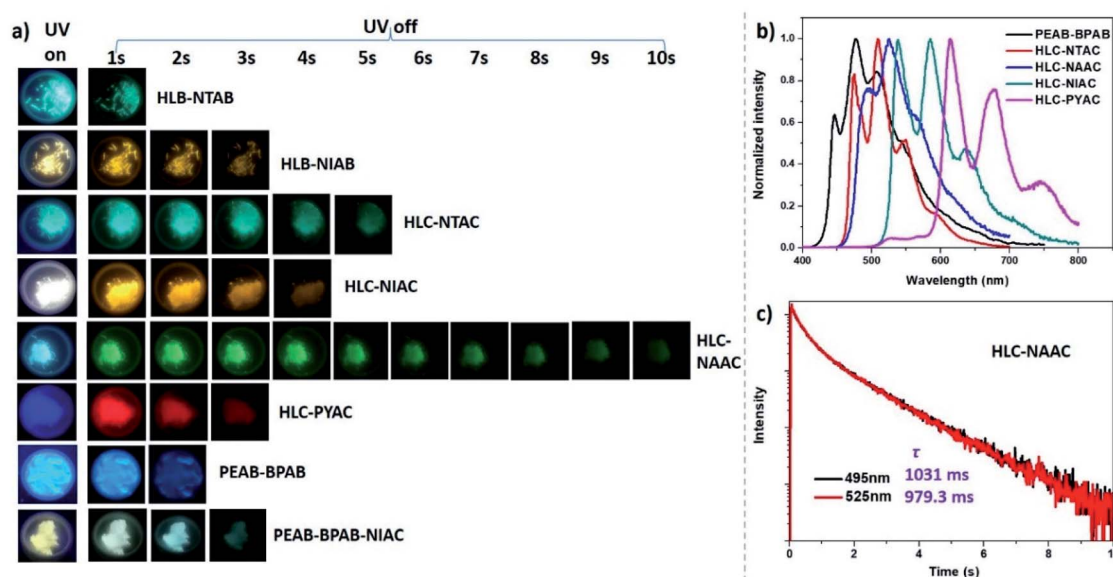

Fig. 5 (a) Afterglow photos of doped halides under a UV lamp of 254 nm (for PEAB–BPAB and PEAB–BPAB–NIAC) and 365 nm (for other halides). (b) Delay emission spectra of PEAB–BPAB, HLC–NTAC, HLC–NAAC, HLC–NIAC and HLC–PYAC. (c) Transient luminescence decay plots of HLC–NAAC monitored at 495 nm and 525 nm.
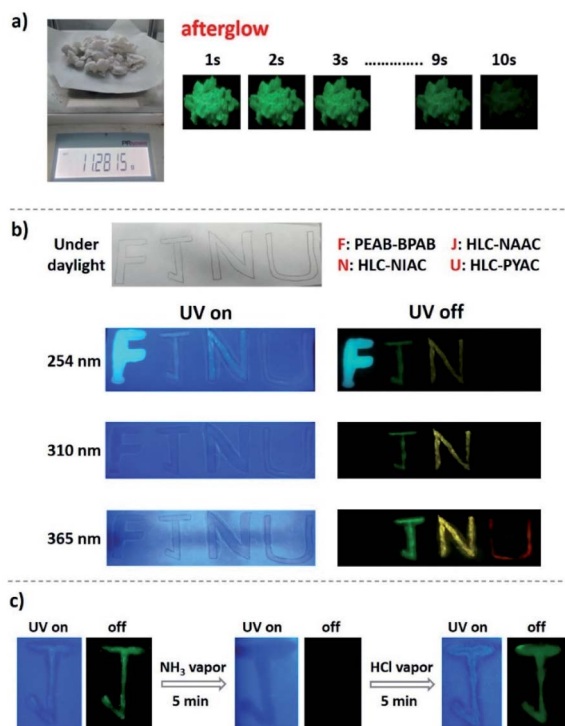
Fig. 6 (a) Photos of 10 g level HLC−NAAC with 10 s of green afterglow. (b) Multiple anti-counterfeiting based on different afterglow colors of PEAB−BPAB, HLC−NAAC, HLC−NIAC and HLC−PYAC inks. (c) Fluorescence/phosphorescence dual responses of HLC−NAAC on both NH₃ and HCl vapors.

stability in air is also important in practical use. Phosphorescent emission of a sample preserved for 12 months in air remains largely the same, which indicates that the RTP of HLC−NAAC is stable under ambient conditions (Fig. S21†). In addition, the RTP stability of HLC−NAAC stored for one year has been measured under a high temperature environment. It was found that the RTP of HLC−NAAC is stable below 175 °C.

With the development of modern science and technology, the requirements for anti-counterfeiting technology in information security have gone higher and higher. Therefore, the exploitation of materials with complex anti-counterfeiting and easy detection technology has always been the focus of information security.[40] These soluble doped halides (such as PEAB−BPAB, HLC−NAAC, HLC−NIAC and HLC−PYAC) with a colorful long afterglow have important application potential in high-level anti-counterfeiting. Firstly, PEAB−BPAB, HLC−NAAC, HLC−NIAC and HLC−PYAC were dissolved in ethanol to form four kinds of safety ink. And then, the four capital letters "FJNU" were written on filter paper with a brush and these safety inks (Fig. 6b). Under a daylight lamp, the color of the four letter is the same as that of the background of the filter paper. When the filter paper is placed under a 254 nm UV lamp, the four letters are distinguished by different colors of fluorescence. After the UV lamp is removed, blue "F", green "J" and yellow "N" letters can be observed due to their different afterglows. When the filter paper is placed under a 310 nm UV lamp, the letters do not show obvious fluorescence. After the UV lamp is removed,

only green "J" and yellow "N" letters can be observed. When the filter paper is placed under a 365 nm UV lamp with high power, the four letters still do not show obvious fluorescence. However, after removing the UV lamp, the three letters of green "J", yellow "N" and red "U" can be seen on the filter paper. Consequently, after being excited by ultraviolet lamps at three different wavelengths, different patterns of fluorescence and afterglow color can be obtained, which increases the level of information anti-counterfeiting. Different from traditional anti-counterfeiting and information encryption materials, these halides are not only easy to synthesize, but are also processed by non-toxic solvent ethanol, which is popular in practical application.

Factory gas leakage is a big problem that must be paid attention to in the chemical industry, because some major safety accidents are often caused by gas leakage that cannot be found in time.[41] NH₃ is an important chemical raw material in chemical production, so the detection of ammonia is particularly important, and the optical response method is a convenient and effective means to detect NH₃.[42] A capital letter "J" was written on filter paper with the HLC−NAAC ink described above. It shows sky-blue fluorescence under a 254 nm UV lamp, and a green afterglow after removing the UV lamp (Fig. 6c). However, both the fluorescence and afterglow disappeared when the filter paper with the letter "J" was fumed with ammonia steam for 5 min. This may be because ammonia destroys the rigid two-dimensional laminate structure of HLC−NAAC, eventually changing the optical properties of HLC−NAAC. Next, the fumed filter paper was used to detect HCl gas. After fuming with HCl gas for 5 min, it was found that both the sky-blue fluorescence and green afterglow of the letter were restored before and after the 254 nm of UV lamp was turned off, respectively. This should be attributed to the consumption of NH₃ by HCl, which restored the layered structure and optical properties of HLC−NAAC. The steam detection method of dual response in terms of fluorescence and phosphorescence further ensures the accuracy of the detection results. In addition, HLC−NAAD can detect NH₃ and HCl at the same time, realizing a double response to both acid and base gases with a single sensor. At present, there are few reports on this kind of sensing material that provides a convenient, fast and efficient new method for steam detection.

Conclusions

In summary, two non-metallic 2D layered organic ammonium salts (HLB and HLC) with ammonium halides as laminates were synthesized. Due to the rigid laminates of the ammonium halides and the external HAE of halogen atoms, HLB and HLC show green room temperature phosphorescence. A series of doped 2D ammonium halide crystals were obtained by doping phosphors (as guests) with different triplet energies into HLB and HLC (as hosts). The visible full-color long afterglow emission of guests was realized by energy transfer between the host and guest. Among them, the phosphorescence quantum yields of green RTP (for HLB−NTAB) and yellow RTP (for HLB−NIAB) are more than 18%. The blue phosphorescence lifetime of PEAC−BPAC synthesized with phenylethylammonium chloride as the host is 1726 ms. When two organic guest ammonium

salts (BPAB and NIAC) were simultaneously doped into phenylethylammonium bromide, a white prompt luminescence and afterglow can be realized. These doped two-dimensional ammonium halides not only show outstanding performance in full-color anti-counterfeiting, but also broader prospects in the fluorescence and phosphorescence two-way detection of acid–base vapor.

Data availability

All data included in this study are available upon request by contact with the corresponding author.

Author contributions

SF and QH designed and carried out the experiments. SF and SY collected and analyzed characterization data. QH and SY analyzed the single crystal structure. SF and ZL wrote the manuscript. ZL and QL supervised the work and gave guidance. All authors have given approval to the final version of the manuscript.

Conflicts of interest

There are no conflicts to declare.

Acknowledgements

Notes and references

1 W. Zhao, Z. He and B. Z. Tang, *Nat. Rev. Mater.*, 2020, **5**, 869–885.
2 Z. Wang, C. Y. Zhu, J. T. Mo, X. Y. Xu, J. Ruan, M. Pan and C. Y. Su, *Angew. Chem., Int. Ed.*, 2021, **60**, 2526–2533.
3 S. Wang, D. Wu, S. Yang, Z. Lin and Q. Ling, *Mater. Chem. Front.*, 2020, **4**, 1198–1205.
4 J. X. Wang, Y. G. Fang, C. X. Li, L. Y. Niu, W. H. Fang, G. Cui and Q. Z. Yang, *Angew. Chem., Int. Ed.*, 2020, **59**, 10032–10036.
5 L. Ma, S. Sun, B. Ding, X. Ma and H. Tian, *Adv. Funct. Mater.*, 2021, **31**, 2010659.
6 T. Zhang, X. Ma, H. Wu, L. Zhu, Y. Zhao and H. Tian, *Angew. Chem., Int. Ed.*, 2020, **59**, 11206–11216.
7 Y. Zhang, C. Liu, H. Zhen and M. Lin, *J. Mater. Chem. C*, 2021, **9**, 5277–5288.
8 Y. Zhou, W. Qin, C. Du, H. Gao, F. Zhu and G. Liang, *Angew. Chem., Int. Ed.*, 2019, **58**, 12102–12106.
9 Q. Huang, X. Mei, Z. Xie, D. Wu, S. Yang, W. Gong, Z. Chi, Z. Lin and Q. Ling, *J. Mater. Chem. C*, 2019, **7**, 2530–2534.
10 Y. Lei, J. Yang, W. Dai, Y. Lan, J. Yang, X. Zheng, J. Shi, B. Tong, Z. Cai and Y. Dong, *Chem. Sci.*, 2021, **12**, 6518–6525.
11 Z. Y. Zhang, W. W. Xu, W. S. Xu, J. Niu, X. H. Sun and Y. Liu, *Angew. Chem., Int. Ed.*, 2020, **59**, 18748–18754.
12 Q. Huang, Z. Lin and D. Yan, *Small Struct.*, 2021, **2**, 2100044.
13 Kenry, C. Chen. and B. Liu, *Nat. Commun.*, 2019, **10**, 2111.
14 R. Gao, M. S. Kodaimati and D. Yan, *Chem. Soc. Rev.*, 2021, **50**, 5564–5589.
15 Z. Wu, J. Nitsch and T. B. Marder, *Adv. Opt. Mater.*, 2021, **9**, 2100411.
16 M. Singh, K. Liu, S. Qu, H. Ma, H. Shi, Z. An and W. Huang, *Adv. Opt. Mater.*, 2021, **9**, 24.
17 S. Guo, W. Dai, X. Chen, Y. Lei, J. Shi, B. Tong, Z. Cai and Y. Dong, *ACS Mater. Lett.*, 2021, **3**, 379–397.
18 Q. Peng, H. Ma and Z. Shuai, *Acc. Chem. Res.*, 2021, **54**, 940–949.
19 Z. Yang, C. Xu, W. Li, Z. Mao, X. Ge, Q. Huang, H. Deng, J. Zhao, F. L. Gu, Y. Zhang and Z. Chi, *Angew. Chem., Int. Ed.*, 2020, **59**, 17451–17455.
20 W. Wang, Y. Zhang and W. J. Jin, *Coord. Chem. Rev.*, 2020, **404**, 213107.
21 H. Shi, Z. An, P.-Z. Li, J. Yin, G. Xing, T. He, H. Chen, J. Wang, H. Sun, W. Huang and Y. Zhao, *Cryst. Growth Des.*, 2016, **16**, 808–813.
22 O. Bolton, D. Lee, J. Jung and J. Kim, *Chem. Mater.*, 2014, **26**, 6644–6649.
23 G. Chen, S. Guo, H. Feng and Z. Qian, *J. Mater. Chem. C*, 2019, **7**, 14535–14542.
24 S. M. A. Fateminia, Z. Mao, S. Xu, Z. Yang, Z. Chi and B. Liu, *Angew. Chem., Int. Ed.*, 2017, **56**, 12160–12164.
25 P. Xue, P. Wang, P. Chen, B. Yao, P. Gong, J. Sun, Z. Zhang and R. Lu, *Chem. Sci.*, 2017, **8**, 6060–6065.
26 S. Yang, D. Wu, W. Gong, Q. Huang, H. Zhen, Q. Ling and Z. Lin, *Chem. Sci.*, 2018, **9**, 8975–8981.
27 S. Yang, B. Zhou, Q. Huang, S. Wang, H. Zhen, D. Yan, Z. Lin and Q. Ling, *ACS Appl. Mater. Interfaces*, 2020, **12**, 1419–1426.
28 Z. A. Yan, X. Lin, S. Sun, X. Ma and H. Tian, *Angew. Chem., Int. Ed.*, 2021, **60**, 19735–19739.
29 H. E. K. El Bahgy, H. Elabd and R. M. Elkorashey, *Environ. Sci. Pollut. Res.*, 2021, **28**, 41431–41438.
30 A. V. Skalny, M. Aschner, I. P. Bobrovnitsky, P. Chen, A. Tsatsakis, M. M. B. Paoliello, A. Buha Djordevic and A. A. Tinkov, *Environ. Res.*, 2021, **201**, 111568.
31 F. Fries, M. Louis, R. Scholz, M. Gmelch, H. Thomas, A. Haft and S. Reineke, *J. Phys. Chem. A*, 2020, **124**, 479–485.
32 B. Ventura, A. Bertocco, D. Braga, L. Catalano, S. d'Agostino, F. Grepioni and P. Taddei, *J. Phys. Chem. C*, 2014, **118**, 18646–18658.
33 Q. Huang, H. Gao, S. Yang, D. Ding, Z. Lin and Q. Ling, *Nano Res.*, 2020, **13**, 1035–1043.
34 G. Tang, K. Zhang, T. Feng, S. Tao, M. Han, R. Li, C. Wang, Y. Wang and B. Yang, *J. Mater. Chem. C*, 2019, **7**, 8680–8687.
35 W. Li, S. Wu, X. Xu, J. Zhuang, H. Zhang, X. Zhang, C. Hu, B. Lei, C. F. Kaminski and Y. Liu, *Chem. Mater.*, 2019, **31**, 9887–9894.
36 K. Jiang, Y. Wang, X. Gao, C. Cai and H. Lin, *Angew. Chem., Int. Ed.*, 2018, **57**, 6216–6220.
37 Q. Huang, S. Yang, S. Feng, H. Zhen, Z. Lin and Q. Ling, *J. Phys. Chem. Lett.*, 2021, **12**, 1040–1045.
38 S. Hirata and M. Vacha, *Adv. Opt. Mater.*, 2017, **5**, 1600996.
39 S. Kuila, S. Garain, S. Bandi and S. J. George, *Adv. Funct. Mater.*, 2020, **30**, 2003693.

40 J. Wang, J. Ma, J. Zhang, Y. Fan, W. Wang, J. Sang, Z. Ma and H. Li, *ACS Appl. Mater. Interfaces*, 2019, **11**, 35871–35878.

41 X.-g. Qi, H. Wang, Y. Liu and G. Chen, *Process Saf. Environ. Prot.*, 2019, **132**, 265–272.

42 X. Li, H. Chen, A. M. Kirillov, Y. Xie, C. Shan, B. Wang, C. Shi and Y. Tang, *Inorg. Chem. Front.*, 2016, **3**, 1014–1020.